SPATIO-TEMPORAL DYNAMICS OF URBAN THERMAL ENVIRONMENT IN UDAIPUR CITY, RAJASTHAN, INDIA

U. Sharma[1], S. Jalan[1*], Y. Kant[2], A. Vyas[3]
[1] Mohanlal Sukhadia University, Udaipur, Rajasthan, India urmisharma2111@gmail.com, seemajalan1@gmail.com
[2] Indian Institute of Remote Sensing, ISRO, Dehradun, India yogesh@iirs.gov.in
[3] L.J. School of Planning, L.J. University, Ahmedabad, India – profanjanavyas@gmail.com

KEY WORDS: Urban Heat Island, NDVI, LST, LULC, Remote Sensing.

ABSTRACT

The Udaipur urban agglomeration was selected to analyse the urban heat island (UHI) effect in the area from 2005 to 2017. Landsat 7 ETM+ sensor data was used to derive land surface temperatures (LST) and map landscape characteristics. The agglomeration was classified into seven land use land cover classes including agriculture cropped, agriculture fallow, barren, built up, scrub, vegetation and water using unsupervised classification method. The LST results were obtained using NDVI method. Urban heat island intensities were mapped using z-score method. Regions with UHI values of above 2 standard deviations were considered to reflect UHI effect. Results show an overall decrease of 10.2 percent in agricultural cropped and fallow lands. The scrub class also shows a moderate decline of 2.3 percent. Increase in area were observed for built up, barren and vegetation classes by 8.8, 2.1 and 1.9 percent respectively. The dominant LULC change was the transformation of agricultural lands to built-up class. The class-wise mean LST observations increase in order of water, vegetation, cropped, fallow, built up, scrub and barren land. The mean LST records an increase of 1.7º C from 30.1º C to 31.8º C over the study period. Results suggest that UHI effects are more prominent in urban fringe area corresponding with the built up and barren land cover classes contrary to its core area. Built up areas surrounded by barren lands left vacant for city's sprawl in the future exhibit highest UHI intensities.

1. INTRODUCTION

Urban areas are expected to absorb virtually all of the future growth of the world's population (United Nations, 2018). The world is expected to have 55 percent of its population living in urban areas, a proportion that is expected to increase to 68% by 2050. This rise in urban population is projected to take place largely in developing nations across Asian and African regions (World Urbanization Prospects, 2018). According to the report India, China and Nigeria will account for 35% of the projected growth of the world's urban population between 2018 and 2050. It is projected that by 2050 India will have added 416 million persons living in urban areas. It has been also projected that growth in Asian countries will be more constrained in the form of growth of medium sized urban centres.

Urbanization as a land surface phenomenon, transforms the natural landscape to anthropogenic urban land and changes surface physical characteristics at local as well as global scales (Huang et al., 2010). In several studies it is seen as the transformation of land uses, previously dedicated largely to agriculture and natural vegetation (Fazal, S., 2000; Malaque, I. R., & Yokohari, M.,2007; Bratley, K., & Ghoneim, E., 2018). The irreversible factor associated with urban landscape dynamics and its negative implications on the environment make it an imperative field of research to prepare grounds for sustainable urban areas (Li et al., 2012; Miller and Small, 2003). Over the past decades, cities in India have urbanized at alarming rates and are likely to be prone to changes in microclimates. The uncontrolled urban growth has taken huge toll over green spaces in these areas and has intensified the UHI effect further. Cities and city regions are sufficiently dense and of a spatial scale that they influence their local micro-climate. (IPCC 6th Assessment Report).

The urban heat island (UHI) effect is one of the widely examined environmental research areas to study the thermal behaviour within cities (Carlson & Aurther, 2000, Weng, Q., Lu, D., & Schubring, J., 2004, Choudhury et al., 2019). The phenomenon is defined as a situation where the temperatures of a city are strikingly high as compared to its neighbouring rural surroundings. The concretization of cities and conversion of agricultural fields to permanent built up regions results into UHI effects. The temperature difference usually is larger at night than during the day, and is most apparent when winds are weak. Seasonally, UHI is seen during both summer and winter. The main cause of the urban heat island is modification of the land surface by urban development which uses materials which effectively retain heat.

A significant component of urban thermal environment studies is surface temperature variation. It is studied as Land Surface Temperature (LST) which modulates the air temperature of lower layer of urban atmosphere and is a primary factor in determining surface radiation and energy exchange, the internal climate of buildings and human comfort in the cities (Voogt & Oke 1998). The satellite derived LST data is used in urban climate and environmental studies, mainly for analysing surface temperature patterns and its relationship with surface characteristics, for assessing UHI and for relating LSTs with surface energy fluxes in order to characterize landscape properties, patterns and processes (Quattrochi and Luvall 1999).

In this context remote sensing technology has great potential for regional planning and urban ecological studies. Remotely sensed imageries with the integration of GIS technology provide an efficient means of obtaining information on temporal trends and spatial distribution of urban areas needed for understanding, modelling and projecting land changes (Owen et al., 1998; Sandholt et al., 2002; Miller and Small, 2003; Voogt and Oke, 2003; Weng et al., 2004; Xiao and Weng, 2007; Xiao et al., 2007; Mallick & Rahman (2012).

A considerable amount of research on UHI have focused largely on municipal areas of big cities. (Grover, A. & Singh, R.B., 2015; Mallick, J., Kant, Y., Bharath, B.D., 2008). However, the

* Corresponding author

horizontal growth of medium size cities has been observed more in peripheral areas lying outside the delimited city area. The consideration of peripheral growth areas witnessing rapid population growth and likely to be engulfed by the delimited municipal area seems to be more useful for sustainable planning of the city. In this context the present study investigates the UHI intensity in Udaipur urban agglomeration area for a period of 12 years from 2005 to 2017. The peripheral areas have noticed tremendous growth during the study period. The rapid growth of the city both horizontally and vertically has resulted into significant changes in land use, increasing its vulnerability to microclimatic changes and UHI effects, possible cause of observed changes in rainfall regime and temperature extremes over past few years.

2. STUDY AREA

Udaipur city is one of the rapidly growing urban centres in southern Rajasthan and part of National Smart Cities Mission initiated by the Government of India. Located at 24º35'N and 73º42'E coordinates the city lies in the foothills of Aravalli range the oldest mountains on earth. It has an average elevation of 598 meters. The city came to its existence in 1559 A.D. for its strategically safe locational site surrounded by Aravallis. The lakes system including three lakes in the upper catchment area, one lake in the downstream, and six lakes within the city makes it the Venice of the East. The city has gained position as top destinations for tourism at global level.

The city has a sub-tropical type of climate. The maximum daily average temperatures recorded for summer and winter seasons are 42° C and 27.5° C respectively. Observations for minimum daily average temperatures for summer and winter seasons are found to be 28° C and 4° C respectively. March to June marks the hot summer season followed by monsoon season of three months from July to September. The cool winter season is starts from October till March characterised by dry conditions mainly except for winter rains from western disturbances. The city receives an average rainfall of about 62.3 cm during monsoon season.

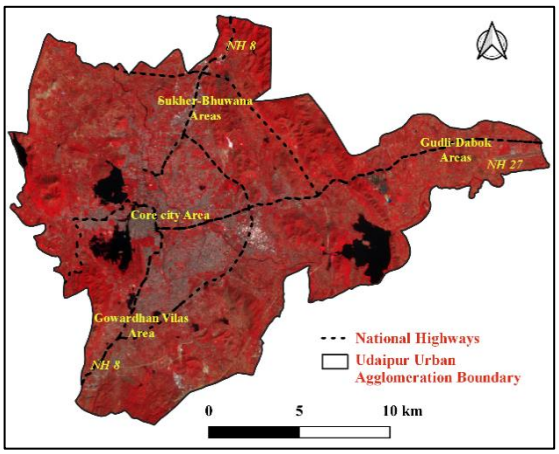

Figure 1. Map of Udaipur Urban Agglomeration.

Urban Improvement Trust (UIT) area also known as Udaipur urban agglomeration (Figure 1) has been selected for the present study to examine the urban heat island intensity in it. It comprises municipal area as well as the planning areas to be developed to facilitate the future growth of the city. It extends across 330.5 square kilometres. The city has recorded a phenomenal population growth rate of 27.6 percent over the period 2011-2023. The current population of the city is estimated as 6.21 lakhs and is expected to reach to more than 10 lakhs by 2031. This increased population leads to areal expansion of city from core to its peripheral parts. The UHI effect is therefore studied in this context to examine the more vulnerable zones of the urban agglomeration.

3. DATA AND METHODOLOGY

3.1 Data

The satellite remote sensing provides vast opportunities to derive land surface characteristics of a region. Further to measure the land surface temperatures and land cover changes for a city area moderate resolution satellite sensors such as Landsat are highly desired. In this study, satellite datasets of Level-1 Precision Terrain (L1TP) of Landsat 7 ETM+ sensor have been obtained from USGS Earth Explorer platform. The main rationale to select this data was its moderate spatial resolution of 30 meter for optical region and 60 meter spatial resolution for thermal bands (available as 30 meter after resampling) considered suitable for time-series analysis. Two sets of satellite data for 2005 and 2017 years with cloud free conditions were acquired for October month.

3.2 Methodology

3.2.1 Data Pre-processing: The datasets obtained were then processed to estimate the thermal intensity as well as landscape characterisation. Landsat 7 scenes collected after 2003 have data gaps due to its Scan Line Corrector (SLC) failure which in the study was corrected for gaps using an add on extension of *landsat_gapfill* of ENVI software for the two scenes. The module provides two ways to perform gap-fill. The single file gap-fill method using a triangulation technique is used in the study.

The atmosphere can affect the quality of remotely sensed images in a number of ways through its components such as oxygen, carbon dioxide, ozone and water vapor. They absorb energy at different wavelengths. The restoration of satellite data from atmospheric effects requires absolute atmospheric correction. This leads to derivation of surface reflectance images using atmospheric correction models. The present investigation used Chavez's Cos(t) model available as one of the ATMOSC models provided by IDRISI Taiga software. It uses a set of atmospheric and viewing condition parameters as input. It incorporates all of the elements of the Dark Object Subtraction model (for haze removal) plus a procedure for estimating the effects of absorption by atmospheric gases and Rayleigh scattering. It requires no additional parameters over the Dark Object Subtraction model and estimates these additional elements based on the cosine of the solar zenith angle (90 – solar elevation). The output in each case is an image of proportional reflectances expressed in real number format as a value ranging between 0.0 to 1. The process was performed on Red and NIR bands of both data sets. The images were then reduced by creating subset of the study area.

3.2.2 Estimation of Land Surface Temperature: To estimate the Land Surface Temperatures (LSTs), NDVI method has been used (Sobrino 2004). The process involves derivation of surface reflectance bands, NDVI, proportionate vegetation, emissivity and land surface temperature results.

Land Surface Temperature (LST) is the radiative skin temperature of the land surface and is an important variable

within the Earth climate system. It is estimated from Top-of-Atmosphere brightness temperatures from the infrared spectral channels of a remote sensing satellite. The theoretical derivation involves following equations to estimate LST on a step-by-step basis and using metadata information of the satellite data.

DN to Radiance conversion:

$$L_\lambda = M_L \times Q_{cal} + A_L \quad (1)$$

where: L_λ is *TOA* spectral radiance (Watts/ ($m^2 \times srad \times \mu m$))
M_L *is b*and-specific multiplicative rescaling factor
A_L is band-specific additive rescaling factor and
Q_{cal} is quantized and calibrated standard product pixel values (DN)

Radiance to Surface Reflectance: Radiance to TOA brightness temperature has been derived using

$$TOA = \frac{K_2}{\ln\left(\frac{K_1}{L_\lambda} + 1\right)} \quad (2)$$

where: TOA is top-of-atmosphere brightness temperature (K)
K_1 & K_2 are band-specific thermal conversion constants 666.09 & 1282.71 (watts/m^2) respectively

Band B6_VCID_2 of Landsat 7 satellite has been used to estimate the land surface temperatures using normalized difference vegetation index (NDVI) threshold methods (Avdan, U., & Jovanovska, G., 2016).

The most important component of retrieving LST is land surface emissivity (LSE). It is a factor that describes how efficiently an object radiates energy as compared to the blackbody (Lillesand, Thomas M., Kiefer, Ralph W., & Chipman, Jonathan W., 2004). Various methods have been used to calculate LSE (Snyder, W. C, Wan, Z., Zhang, Y., & Feng, Y.Z., 1998; Peres, L. F., & DaCamara, C.C., 2004; Li, Z. L., et. al., 2013). NDVI threshold method is used here which assumes that the surface component is made of a mixture of bare soil and vegetation (Sobrino, J. A., et. al., 2008; Valor, E., & Caselles, V., 1996; Peres, L. F. , & DaCamara, C.C.; 2005; Yamamoto, Y. , & Ishikawa, H.; 2017). The process of estimating LSE has been elaborated in following sub-sections:

Calculating Normalized Difference Vegetation Index (NDVI): NDVI is one of the popular vegetation indices derived using satellite data to estimate the healthiness of the vegetation. NDVI has been calculated as:

$$NDVI = (NIR - Red)/(NIR + Red) \quad (3)$$

where: *NIR* is the near infrared band (band 4) and
Red is red band (band 3) of Landsat 7 satellite data

Calculating Proportionate Vegetation Index (Pv):Pv is the vegetation proportion viewed by the sensor and is obtained using Carlson, T. N., & Ripley, D. A., 1997 method.

$$Pv = \left[\frac{NDVI - NDVI\,min}{NDVI\,max - NDVI\,min}\right]^2 \quad (4)$$

where: NDVI *max* is for vegetation
NDVI *min* is for bare ground

Calculating land surface emissivity ($\mathcal{E}$): The pixel-wise land surface emissivity is calculated as:

$$\mathcal{E} = \mathcal{E}v\,Pv + \mathcal{E}s\,(1 - Pv) + d\mathcal{E} \quad (5)$$

where: $\mathcal{E}v$ = 0.9863 and $\mathcal{E}s$ = 0.9668 are the emissivities of the vegetation and soil
$d\mathcal{E}$ = 0.004 (approximation)

$d\mathcal{E}$ is the mean weighted value that takes into account the mean of emissivity value of different surface types (Mallick, J., Kant, Y., & Bharat, B., 2008). The emmisisivity for pixels over water areas has been set to 0.99 in the calculation.

Calculating land surface temperature (LST):

$$LST = \frac{\mathrm{TOA}}{\left\{1 + \left[\left(\lambda * \mathrm{TOA}/\rho\right)\ln \mathcal{E}\right]\right\}} - 273.15 \quad (6)$$

where: TOA is at-sensor brightness temperature (in kelvin),
λ is the wavelength of emitted radiance (for which the peak response and the average of the limiting wavelengths =11.35 μm) (Band 6_VCID_2)
$\mathcal{E}$ is the emissivity calculated in (5) and
$\rho = h \times c/\sigma = 1.438 \times 10^{-2}$ mK, which is further converted to μm units before putting into the equation (6)
h is Planck's constant (6.626×10^{-34} Js)
σ is the Boltzmann constant (1.38×10^{-23} J/K)
c is the velocity of light (2.998×10^8 m/s)

3.2.3 Land Use Land Cover Classification: The K-means unsupervised classification method with a maximum of 10 iterations was used to classify the study area. Seven land cover classes have been selected on the basis of National Remote Sensing Centre (NRSC), Hyderabad level 1 classification scheme for the present research. The classes are namely: *agriculture cropped, agriculture fallow, barren, built-up, scrub, vegetation and water*. *Water* includes rivers, lakes and tanks filled with water. *Scrub* includes mostly dry shrubs over a piece of land. *Barren* has been referred to as either rocky topography or area often devoid of vegetation cover. A *built-up* area is defined as an area of human habitation developed out of non-agricultural use of the land and that has a cover of buildings transport and communication utilities. It also includes mining areas in the present study. The *vegetation* includes areas with trees and grass i.e., green land cover which is not agriculture. The class includes vegetation in forest region, plantation along roadside, public parks, and gardens in cities. The *agriculture cropped* refers to the land cover which has standing crop at the time of satellite pass. The *agriculture fallow* includes temporarily uncropped cultivable land. This understanding of *agriculture* land cover including both cropped and fallow has been considered in context of date of satellite overpass during data collection. To improve the classified results post-classification recoding was performed. A stratified random sampling method was applied to choose 50 samples in every LULC category. The overall accuracy was observed to be more than 85% for both years.

3.2.4 Estimation of Urban Heat Island: LST results were used to analyse the urban heat island effect in the study area by calculating statistical z-score. The UHI is calculated using following equation:

$$UHI = (Ts - Tm)/SD \quad (7)$$

where: Ts is Land surface temperature
Tm is the mean LST of the area
SD is the standard deviation

The UHI derived for each dataset has been classified into six classes of *below -2 SD, -2 to -1 SD, -1 to 1 SD, 1 SD to 2 SD, 2 SD to 3 SD* and *above 3 SD* to observe variations in UHI effect across the area.

To correlate the LST, NDVI, UHI and LULC results a fishnet grid of 100 by 100 meters cell size was generated for both scenes in ArcGIS software. Total 4851 centroid points were created using this fishnet to extract pixel values of all four variables each for 2005 and 2017.

4. RESULTS

4.1. Spatio-Temporal Analysis of Land Use Land Cover

The classified images were compared in relation to their total area under each land cover class. Table 1 shows that classes that have decreased in area include agriculture cropped, scrub, agriculture fallow and water. An overall decrease of 10.2 percent is observed for total agricultural area comprising of agricultural cropped and fallow lands over the study period. The scrub class show a moderate decline of 2.3 percent while least area change is found for water class by decrease of 0.3 percent. The classes that have increased in area are built-up, barren and vegetation with an increase in area by 8.8, 2.1 and 1.9 percent respectively.

Land Use Land Cover	*Area 2005 (in %)*	*Area 2017 (in %)*	*Change in area (in %)*
Agriculture Cropped	32.9	24.4	-8.5
Agriculture Fallow	10.6	8.9	-1.7
Barren	17.4	19.5	2.1
Built up	16.4	25.2	8.8
Scrub	6.7	4.5	-2.3
Vegetation	11.1	13.0	1.9
Water	5.0	4.6	-0.3

Table 1. Percent area under different LULC classes and change in area from 2005 to 2017

In Figure 2 spatial patterns of LULC results exhibit that the urban built up shows radial growth outwards in three directions from city core. It extends in north, east and southern parts of the city along major highways. The area of built up has grown tremendously in 2017 within the urban limit. The phenomenal urban growth is observed more in peripheral areas of the core city. It extends outward along National Highway 8 in both north and south directions. The eastern part of the city exhibits ribbon growth along National Highway 27 comprising mainly the industrial areas of Umarda, Gudli and Dabok. Scattered growth is found over northern and southern ends. This increase corresponds to the transformation of agricultural lands into built up classes. The vegetation class is found mainly over hilly parts of the city distributed in the north-east, west and south of the study area. The topographical constraint restricts the city growth in the west direction. Another transformation of areas of barren cover to urban built up are seen in the peripheral region in north-west, southern and eastern parts of Udaipur. However, increase in barren area corresponds to the new areas marked for future development of the city. Marginal land cover classes namely vegetation and scrub show interchanging distribution in tandem with the prevalent climatic conditions at the time of satellite pass. The water classes are found largely comprising major lakes and Ayad river in the area.

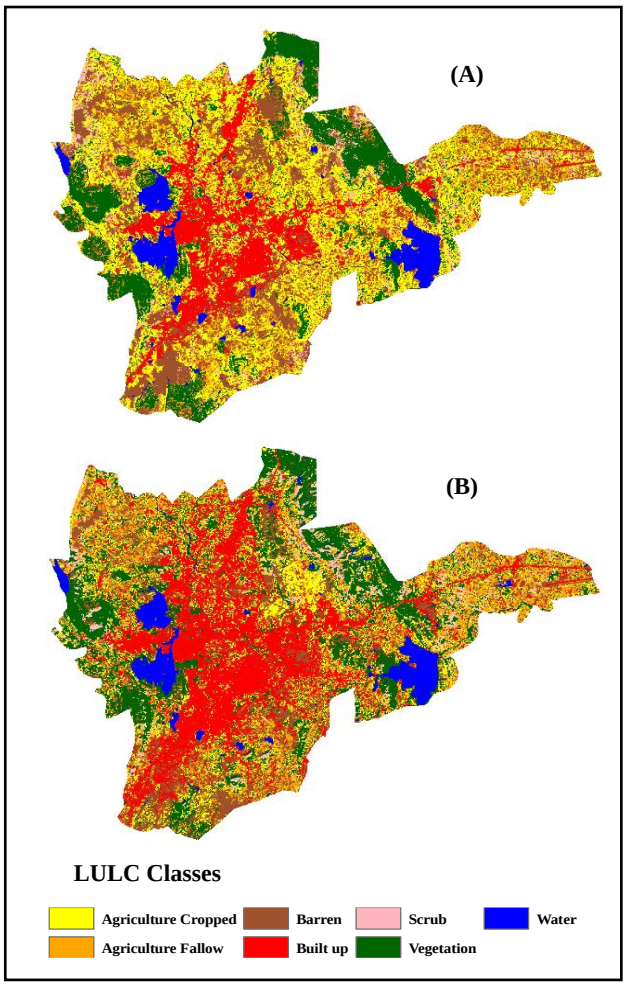

Figure 2. LULC maps for (A) 2005 and (B) 2017

4.2 Spatio-Temporal Analysis of Land Surface Temperatures

The overall mean LST records an increase of 1.7º C from 30.1º C to 31.8º C over 2005-2017. The class-wise mean LST as seen in Table 2 shows that maximum temperatures are recorded over barren class with 31.9º C followed by scrub with 31.4º C, built up with 31.3º C, agriculture fallow with 31.1º C, agriculture cropped with 30.4º C. The low mean LST are recorded for vegetation with 28.3º C and minimum over water with 24.6º C for 2005. Similarly, for 2017 trends of mean LST follow barren with 31.8º C, scrub with 31.7º C, built up with 31.5º C, agriculture fallow with 31.4º C and agriculture cropped with 31.1º C temperatures. Observations for lower LST are recorded over vegetation with 29.4º C and water with 25.8º C.

Spatial patterns of LST show an overall increase in temperatures in the city area. Figure 3 shows that concentration of high LST regions is found over peripheral areas in the east and southern part of the city. These areas correspond to the barren and scrub classes in the east and built up class in the south. In northern part high LST areas also coincide with barren, scrub and built up land

covers. Lower LST areas correspond to the vegetation and water classes for both scenes. It is noted that they show maximum increase in the mean LST among other LULC classes.

Land Use Land Cover	*Mean LST (° C) 2005*	*Mean LST (° C) 2017*
Agriculture Cropped	30.4	31.1
Agriculture Fallow	31.1	31.4
Barren	31.9	31.8
Built up	31.3	31.5
Scrub	31.4	31.7
Vegetation	28.3	29.4
Water	24.6	25.8

Table 2. Class-wise mean LST for 2005 & 2017

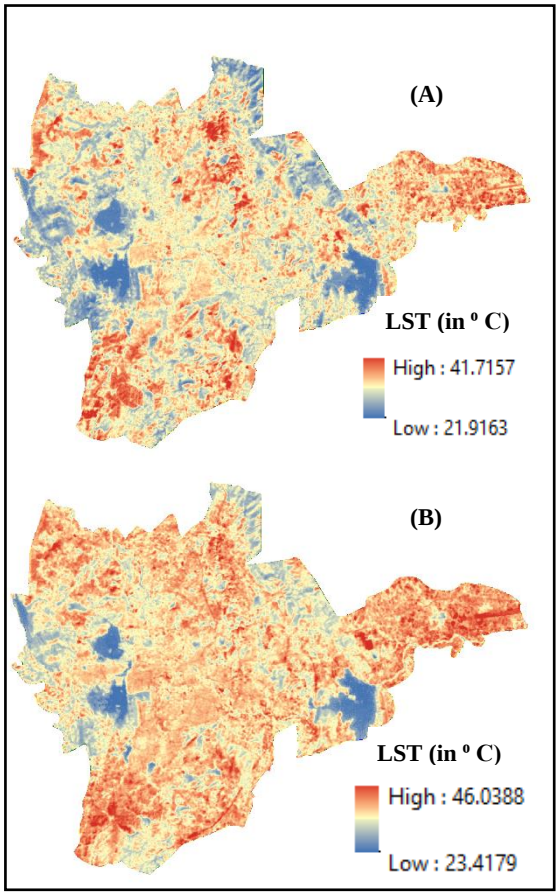

Figure 3. LST maps for (A) 2005 and (B) 2017

4.3 Spatio-Temporal Analysis of Urban Heat Island Effect

To estimate the impact of urban heat island effect in the study area UHI maps were generated. The UHI values with Z-Score higher than 2 have been considered as exhibiting high UHI intensity or the presence of heat island effect. UHI effects were recorded over higher LST areas in eastern and southern parts of the city as shown in Figure 4.

The decrease in UHI intensity from 2005 to 2017 in the northern part corresponds to conversion of barren lands to built up areas over the study period. In contrast to the concept of UHI phenomenon where inner temperatures of a city are found higher the core of Udaipur city exhibits no UHI effect in it. Distinctively the peripheral areas show effect of UHI corresponding to the prevailing land covers in both scenes. The spatial patterns also reveal an increasing trend in UHI intensity in the western part where new built up and barren lands are emerging over vegetation and cropped covers.

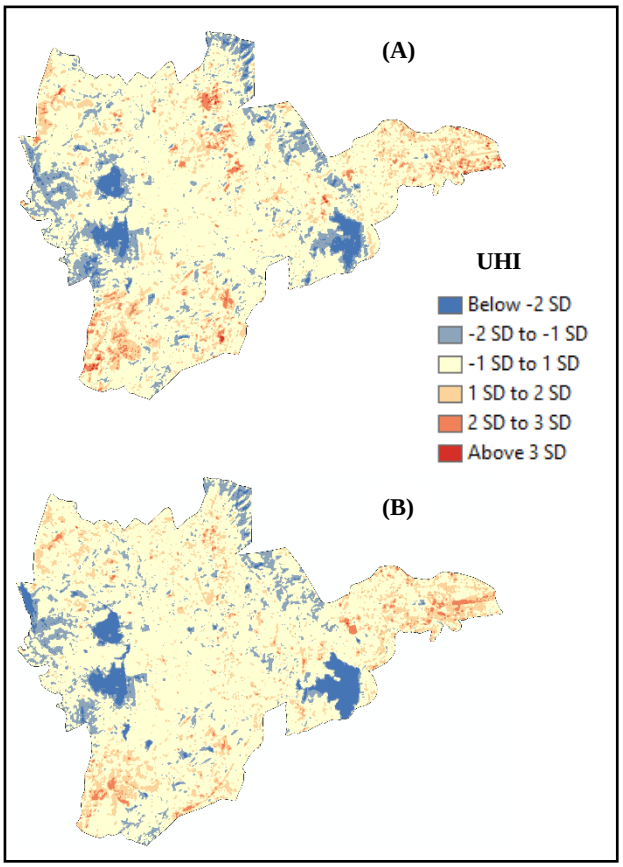

Figure 4. UHI intensities for (A) 2005 and (B) 2017

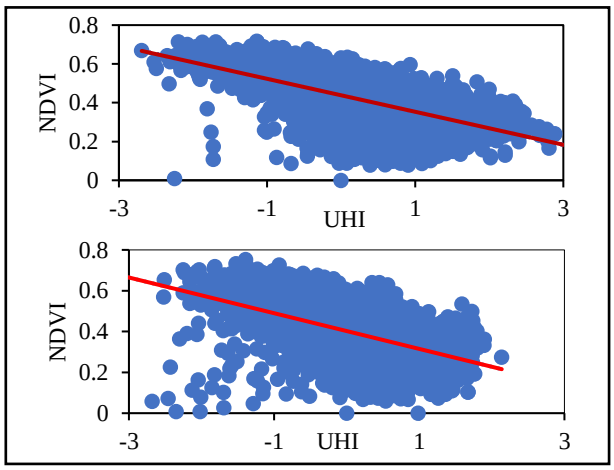

Figure 5. Scatter plots of UHI and NDVI 2005 and 2017

To analyze the UHI intensity in context of green areas a comparison between UHI and NDVI observations was made. The fishnet point data has been used to generate scatter plots of UHI and NDVI for 2005 and 2017 in Figure 5. This analysis excluded the NDVI values of water class as they are negative. A negative correlation of -0.55 for 2005 and -0.50 for 2017 for UHI and NDVI were observed.

5. CONCLUSIONS

The increase in population of Udaipur agglomeration is depicted in the changing spatial patterns of LULC. The dominant change is observed in the transformation of agricultural lands to built-up class. Results suggest that UHI effects are more prominent in urban fringe area of Udaipur urban agglomeration. The UHI pattern coincides effectively with increase in built up areas and corresponding barren and scrub lands. This fringe area consists of marble industrial regions extended in Sukher-Bhuwana areas along NH 8 in north. The industrial regions of Debari and Gudli-Dabok represent UHI affected areas in eastern fringe zone. The results also manifest that not only industrial but the new residential areas developed under planning initiatives by the government comprising Bhuwana in north, Ambamata in west, Hiran Magri, Govardhan Vilas in the south and Umarda-Gudli-Dabok in the east are vulnerable to the UHI effect. A declining trend of UHI reflects transformation of high LST barren areas to built up class exhibiting comparatively lower LST values. Western part of the city notably shows increasing trend in UHI intensities conforming with the growth of built up area in this part. The results of correlation between UHI and NDVI are suggestive of managing green spaces in peripheral areas of the Udaipur urban agglomeration to control the emerging UHI effects.

6. REFRENCES

ArcGIS [GIS software]. Version 10.0. Redlands, CA: Environmental Systems Research Institute, Inc., 2010.

Avdan, U., & Jovanovska, G., 2016. Algorithm for Automated Mapping of Land Surface Temperature Using LANDSAT 8 Satellite Data. *Journal of Sensors*.

Bratley, K., & Ghoneim, E., 2018. Modeling Urban Encroachment on the Agricultural Land of the Eastern Nile Delta Using Remote Sensing and a GIS-Based Markov Chain Model. *Land*, 7(4), 114.

Carlson, T. N., & Arthur, S. T., 2000. The impact of land use — land cover changes due to urbanization on surface microclimate and hydrology. a satellite perspective. *Global and Planetary Change*, 25(1–2), 49–65.

Carlson, T. N., & Ripley, D. A., 1997. On the relation between NDVI, fractional vegetation cover, and leaf area index. *Remote Sensing of Environment*, 241– 252.

Census of India, 2011. Ministry of Home Affairs. Government of India, New Delhi.

Choudhury, D., Das, K., & Das, A., 2019. Assessment of land use land cover changes and its impact on variations of land surface temperature in Asansol-Durgapur Development Region. *The Egyptian Journal of Remote Sensing and Space Science*, 22(2), 203–218.

Clark Labs, Clark University, 2009. IDRISI Taiga (16.04) [Software].

Fazal, S., 2000. Urban expansion and loss of agricultural land - a GIS based study of Saharanpur City, India. *Environment and Urbanization*, 12(2), 133–149.

Grover A, & Singh, R.B., 2015. Analysis of Urban Heat Island (UHI) in Relation to Normalized Difference Vegetation Index (NDVI). A Comparative Study of Delhi and Mumbai. *Environments*. 2(2).125-138.

Jensen, J. R. (1996). Introductory digital image processing (3rd ed.) Upper Saddle River, NJ. Prentice Hall.

Landsat-7 image courtesy of the U.S. Geological Survey

Li, Z. L., Wu, H., Wang, N., Qiu, S., Sobrino, J. A., Z. Wan, . . . G. Yan., 2013. Land surface emissivity retrieval from satellite data. *International Journal of Remote Sensing*, 3084 - 3127.

Lilesand, Thomas M., Kiefer, Ralph W., & Chipman, Jonathan W., 2004. *Remote Sensing and Image Interpretation.* Wiley India.

Malaque, I. R., & Yokohari, M., 2007. Urbanization process and the changing agricultural landscape pattern in the urban fringe of Metro Manila, Philippines. *Environment and Urbanization*, 19(1), 191–206).

Mallick, J., & Rahman A., 2012. Impact of population density on the surface temperature and micro-climate of Delhi. *Current Science*. 12 (102), 1708-1713.

Mallick, J., Kant, Y., & Bharath, B.D., 2008. Estimation of land surface temperature over Delhi using Landsat-7 ETM. *The Journal of Indian Geophysical Union*.12, 131–140.

Miller, R.B., Small, C., 2003. Cities from space. potential applications of remote sensing in urban environmental research and policy. *Environ. Sci. Policy*. 6, 129–137.

Owen, T.W., Carlson, T.N., Gillies, R.R., 1998. An assessment of satellite remotely-sensed land cover parameters in quantitatively describing the climatic effect of urbanization. *Int. J. Remote Sensing*. 19, 1663–1681.

Peres, L. F. , & DaCamara, C.C., 2005. Emissivity maps to retrieve land-surface temperature from MSG/SEVIRI. *IEEE Transactions on Geoscience and Remote Sensing*, 1834 –1844.

Peres, L. F., & DaCamara, C.C., 2004. Land surface temperature and emissivity estimation based on the two-temperature method. Sensitivity analysis using simulated MSG/SEVIRI data. *Remote Sensing of Environment*, 377–389.

Quattrochi, D.A., & Luvall, J.C., 1999. Thermal infrared remote sensing for analysis of landscape ecological processes. Methods and applications. *Landscape Ecology*, 14 (6), 577-598.

Sandholt, I., Rasmussen, K., Anderson, J., 2002. A simple interpretation of the surface temperature/vegetation index space for assessment of surface moisture status. *Remote Sensing Environ.* 79, 213–224.

Snyder, W. C, Wan, Z., Zhang, Y., & Feng, Y.Z.; 1998. Classification-based emissivity for land surface temperature measurement from space. *International Journal of Remote Sensing*, 2753 - 2774.

Sobrino, J. A., et. al., 2008. Land surface emissivity retrieval from different VNIR and TIR sensors. *IEEE Transactions on Geoscience and Remote Sensing*, 316–327.

Sobrino, J. A., Jiménez-Muñoz, J. C., & Paolini, L., 2004. Land surface temperature retrieval from LANDSAT TM 5. *Remote Sensing of Environment*, 90(4), 434–440.

United Nations, Department of Economic and Social Affairs, Population Division, 2019. World Urbanization Prospects. The 2018 Revision (ST/ESA/SER.A/420). New York. United Nations.

United Nations. (2021). IPCC Sixth Assessment Report.

Valor, E., & Caselles, V., 1996. Mapping land surface emissivity from NDVI. Application to European, African, and South American areas. *Remote Sensing of Environment*, 57, 167–184,, 167 - 184.

Voogt, J.A., Oke, T.R., 2003. Thermal remote sensing of urban climates. *Remote Sensing Environ*. 86, 370–384.

Weng, Q., Lu, D., & Schubring, J., 2004. Estimation of land surface temperature–vegetation abundance relationship for urban heat island studies. *Remote Sensing of Environment*, 89(4), 467–483.

Weng, Q., Lu, D., Schubring, J., 2004. Estimation of land surface temperature–vegetation abundance relationship for urban heat island studies. *Remote Sensing Environ*. 89, 467–483.

Xiao, H., & Weng, Q., 2007. The impact of land use and land cover changes on land surface temperature in a karst area of China. *J. Environ. Manage*. 85, 245– 257.

Xiao, R., et. al., 2007. Spatial pattern of impervious surfaces and their impacts on land surface temperature in Beijing, China. *J. Environ. Sci*. 19, 250–256.

Yamamoto, Y. , & Ishikawa, H., 2017. Thermal Land Surface Emissivity for Retrieving Land Surface Temperature from Himawari-8. *Journal of Meteorological Society of Japan*.